EXPERIMENTAL EVALUATION OF SAMPLING BIAS IN INDIVIDUAL REALIZATION LASER ANEMOMETRY

By

MICHAEL SCOTT QUIGLEY

Bachelor of Science

Oklahoma State University

Stillwater, Oklahoma

1974

Submitted to the Faculty of the
Graduate College of the
Oklahoma State University
in partial fulfillment of
the requirements for
the Degree of
MASTER OF SCIENCE
December, 1975

EXPERIMENTAL EVALUATION OF SAMPLING
BIAS IN INDIVIDUAL REALIZATION
LASER ANEMOMETRY

Thesis Approved:

W. G. Tiederman Jr.
Thesis Adviser

D K McLaughlin

J. A. Uhlbelt

N M Durham
Dean of the Graduate College

ACKNOWLEDGMENTS

A special thanks goes to my thesis adviser, Dr. W. G. Tiederman, who was mainly responsible for shaping my concepts about fluid dynamics research. I sincerely appreciate all the guidance and criticism he and Dr. D. K. McLaughlin, another major influence on my research technique, gave me during the course of this study.

I am also very grateful to my wife, Kathy, who typed the rough draft, helped me with a data run, and encouraged me to continue when my research and experiments seemed to go wrong.

I owe a debt of gratitude to many other people, especially those on the BFDL research team. My thanks to Afshin Ghajar, Alan Smith, Greg Shedeck, Nader Sharabianlou, and David Bogard for helping with data runs and keeping me company at the Bar Ditch. I also want to thank David Bogard for his technical assistance and electronics expertise and for the many good ideas he gave me during the course of this study. Dean Quigley, in Seattle, Washington, deserves a special thanks for his emergency purchase of Tally mechanism oil.

Finally, I am especially grateful to Velda Davis for typing and managing the final draft of this thesis.

TABLE OF CONTENTS

LIST OF TABLES

LIST OF FIGURES

NOMENCLATURE

D_H	Hydraulic diameter, inches
F	Doppler frequency, Hz
h	Height, inches
L	Length between pressure taps, inches
N	Number of realizations
P	Pressure
$\dot{Q}$	Flow rate, gallons per minute
R_{12}	Velocity correlation, $\frac{\overline{uv}}{u'v'}$
S	Fringe spacing, μm
SG	Specific gravity
T	Integration time
T_D	Doppler period, seconds
U	Velocity, ft/sec
$\overline{U}_a$	Mass average velocity, ft/sec
$\overline{U}_c$	Period average velocity, ft/sec
$\overline{U}_e$	Frequency average velocity, ft/sec
U_i	An individual velocity realization, ft/sec
U^+	Non-dimensional streamwise velocity
u_τ	Shear velocity, ft/sec
u'	RMS, streamwise velocity fluctuation - unweighted average
u'_m	RMS Streamwise velocity fluctuation - weighted average

u_o'	RMS fluctuation corrected for biasing and finite probe volume effects
$\tilde{V}_i$	Average velocity over Δt_i, ft/sec
$\overline{V}, \tilde{V}$	Time average velocity, ft/sec
w	Probe volume width, inches
y	Distance normal to wall, inches
y^+	Non-dimensional y location
Δt_i	Time between realizations
$\frac{\Delta \overline{U}}{\Delta y}$, b	Slope of the average velocity profile, $\frac{ft/sec}{in}$
Δ	Change in a quantity
$\theta/2$	Beam intersection half-angle
λ	Wavelength of laser light
μ	Absolute viscosity, $\frac{lbm}{ft\ sec}$
ν	Kinematic viscosity, $\frac{ft^2}{sec}$
ρ	Density, $\frac{lbm}{ft^3}$
ρ_s	Seed concentration, gm/250 gal
τ_w	Wall shear stress, $\frac{lb_f}{ft^2}$
ω_i	Weighting function

CHAPTER I

INTRODUCTION

The basic principle of laser Doppler anemometry is a well understood, much-explained phenomenon. Simply put, a light-scattering particle passing through the fringe pattern created by crossing two coherent, plane polarized light beams modulates the reference light frequency with a characteristic Doppler frequency. This Doppler frequency shift is equal to the component of particle velocity normal to the fringes, U, divided by the fringe spacing, S. The relationship is

$$U = FS = \frac{F\ \lambda}{2\ \sin\ (\frac{\theta}{2})} \qquad (1\text{-}1)$$

where F is the Doppler frequency, λ is the reference light wavelength, and $(\frac{\theta}{2})$ is the beam intersection half-angle. If the light-scattering particle is entrained in a fluid and accurately follows the fluid motion, a measurement of the fluid velocity can be made at the probe volume formed at the beam's intersection.

Individual Realization Anemometer

Whenever a seed particle passes through the probe

volume an individual realization of the fluid velocity occurs. The mode of operation of the laser Doppler anemometer used in this study is based on this principle of individual velocity realizations. This mode of operation occurs when the flow is so lightly seeded with scattering centers that in any instant there is at most one particle in the probe volume. Typically, particles are in the probe volume less than 4% of the time, which corresponds to a low duty cycle. Here duty cycle is the ratio of the time spent in the probe volume to the total time. The mean velocity is statistically calculated from a histogram of these individual realizations in addition to any other desired velocity information. The difficulty with this approach for turbulent flows is that analyses have suggested that the simple ensemble average of the realizations

$$\overline{U}_e = \frac{1}{N} \sum_{i=1}^{N} U_i \qquad (1\text{-}2)$$

provides a higher estimate of the mean velocity than the normally required time average velocity

$$\overline{U} = \frac{1}{T} \int_t^{t+T} U(t)dt. \qquad (1\text{-}3)$$

The biasing occurs because the probability of a realization occurring is proportional to the instantaneous velocity. This statistical biasing has been proposed and analyzed by McLaughlin and Tiederman (1973) and Barnett and Bentley (1974), but its existence has not been experimentally

verified. Moreover, there is some disagreement as to how the duty cycle effects the biasing and this leads to different conclusions about when a correction should be made to the data.

Objective

With the diverse and widespread use of laser anemometers, the precise interpretation of their data is becoming crucial. The rapidly growing need for more accuracy demands that the biasing issue be resolved as quickly and as completely as possible. The focal point of this study was to experimentally test the proposed biasing corrections for individual realization anemometer data. The experiments were conducted in the viscous sublayer of a two-dimensional turbulent channel flow of water. The objective was to compare the slope of the viscous sublayer profile measured by the laser anemometer to the slope of the velocity profile calculated from simultaneous measurements of the pressure gradient. The number density of the light-scattering seed particles in the water was low enough to assure duty cycles less than 4%.

CHAPTER II

STATISTICAL BIASING

The Occurrence of Biasing

One of the principle quantities of interest in fluid flow measurements is the time average velocity at a point as given by Equation (1-3). For an unbiased histogram of random, independent velocity realizations this is simply the ensemble average of the realizations given by Equation (1-2). Although an individual realization is a random event in time for a uniform seed distribution, the possibility of occurrence is proportional to the instantaneous flow velocity (see McLaughlin and Tiederman, 1973) because the probability of obtaining a velocity realization is proportional to the volume of fluid flowing through the probe volume. Thus, for highly turbulent flows $\overline{U}_e > \overline{U}$ because a higher than average number of scattering centers pass through the probe volume during periods when the velocity is greater than $\overline{U}$. The converse occurs when the velocity is smaller than $\overline{U}$. The result is obviously more high velocity realizations than low, and statistics that are biased high. The magnitude of this statistical biasing can be as much as 10% for flows having turbulent intensities of 30% or more (Karpuk, 1974, and

McLaughlin and Tiederman, 1973). Herein lies the problem of correctly interpreting individual realization laser anemometer data for turbulent flows.

Statistical Biasing Corrections

McLaughlin and Tiederman (1973) propose that a properly weighted ensemble average

$$\overline{U} = \frac{\sum_{i=1}^{N} \omega_i U_i}{\sum_{i=1}^{N} \omega_i} \qquad (2\text{-}1)$$

will yield a good estimate of the time average velocity. Central to the foregoing are three basic assumptions: (1) the particles are small enough to follow the mean flow accelerations as well as the fluctuations associated with turbulence. (2) The particles are randomly distributed with respect to number density in the stationary make up fluid. (3) The flow is so lightly seeded that the swept volume is much greater than the volume of the probe volume. The third assumption indicates that the average number of realizations obtained per unit time is proportional to the magnitude of the velocity vector.

Using these assumptions, the proper weighting function, ω_i, was deduced to be the inverse of the instantaneous velocity vector. However, for most flow situations, it was postulated that a simplified correction based on the streamwise velocity component would be adequate. Consequently,

$$\overline{U}_c = \frac{\sum_{i=1}^{N} \left(\frac{1}{U_i}\right) U_i}{\sum_{i=1}^{N} \left(\frac{1}{U_i}\right)} \tag{2-2}$$

which simplifies to

$$\overline{U}_c = \frac{N}{\sum_{i=1}^{N} \left(\frac{1}{U_i}\right)}. \tag{2-3}$$

Since U_i is directly proportional to the Doppler period, T_D, it is quite straightforward to calculate the corrected mean velocity based on the average Doppler period, $\overline{T}_D$, such that

$$\overline{U}_c = \frac{S}{\overline{T}_D} = \frac{\left[\frac{\lambda}{2} \sin\left(\frac{\theta}{2}\right)\right]}{\overline{T}_D} \tag{2-4}$$

This period average velocity is the biased-corrected velocity of Equation (2-3).

McLaughlin and Tiederman (1973) applied the one-dimensional biasing correction scheme to several assumed flow models of fully developed pipe flow. Their analytical results clearly show the effects of statistical biasing on the mean and fluctuating velocity components. Moreover, the results were compatible with the original assumption of low seed particle density necessary for individual realization measurements. They do not indicate any dependence on duty cycle other than the basic individual realization requirement.

The biasing correction proposed by Barnett and Bentley

(1974) is similar to the technique described above in assuming constant particle density but differs in one major aspect. It specifies the velocity changes in the probe volume be strongly correlated with those immediately upstream. If this is the case, then it can be shown that the time interval between successive realizations, Δt_i, must be inversely proportional to the average fluid velocity, $\tilde{V}_i$, over the interval.

Once again the time average velocity is the quantity of interest. Using the nomenclature of Barnett and Bentley (1974)

$$\tilde{V} = \frac{1}{T} \int_0^T V(t)dt \qquad (2\text{-}5)$$

where $\tilde{V}$ is the temporal mean (time average) of velocity. Because particles are not continuously in the probe volume, data are not continuously taken and Equation (2-5) was approximated by

$$\overline{V} = \frac{1}{T} \sum_{i=1}^{M} V_i \Delta t_i . \qquad (2\text{-}6)$$

Taking into account

$$T = \sum_{i=1}^{M} \Delta t_i \qquad (2\text{-}7)$$

the temporal mean becomes

$$\overline{V} = \frac{\sum_{i=1}^{M} \frac{V_i}{\tilde{V}_i}}{\sum_{i=1}^{M} \frac{1}{\tilde{V}_i}} \qquad (2\text{-}8)$$

The result is the same as the McLaughlin-Tiederman biasing correction except that $\tilde{V}_i$ is the average probe volume velocity in the time between realizations instead of the instantaneous velocity, U_i. From Equation (2-8) and a series expansion of Equation (2-5), Barnett and Bentley conclude that when the sampling frequency is much less than the frequency of flow oscillations, $\tilde{V}_i$ approaches the mean fluid velocity, $\tilde{V}$. This is the case of low duty cycle for which Δt_i is essentially constant and the time average and ensemble average are the same. This infers that there is no correlation between the instantaneous velocity and the sampling rate. Therefore, no statistical biasing of the data occurs.

Conversely when the duty cycle is relatively high for individual realization anemometry the sampling rate is much greater than the frequency of the flow oscillations and $\tilde{V}_i \simeq V_i$. For this case the result

$$\overline{V} = \frac{M}{\sum_{i=1}^{M} \left(\frac{1}{V_i}\right)} \qquad (2\text{-}9)$$

agrees with the biasing correction proposed by McLaughlin and Tiederman (1973) shown in Equation (2-3).

Although these two sets of analyses do not reach the same conclusions with respect to duty cycle effects, both demonstrate that when statistical biasing occurs it creates a significant error in the measurement of the mean and fluctuating velocity. Tiederman, McLaughlin, and Reischman

(1973), Karpuk (1974), and Reischman and Tiederman (1974) applied the one dimensional biasing correction proposed by McLaughlin and Tiederman (1973) to their individual realization measurements in two-dimensional turbulent channel flows of water and dilute polymer solutions. Their data demonstrate that the biasing correction can lower the estimate of the mean velocity by about 10% and the estimate of streamwise turbulent intensity by as much as 100%. Thus, it is extremely important to experimentally verify the existence of statistical biasing and determine whether or not it is a function of duty cycle. Moreover, it is desirable to establish a proper correction scheme for individual realization measurements. This study was undertaken for these two reasons.

CHAPTER III

EXPERIMENTAL TECHNIQUES AND APPARATUS

Overall Technique

In order to examine the effects of biasing on the mean velocity, it is necessary to compare the laser anemometer data against an independent measurement. The quantity of interest is the slope of the velocity profile at the wall of the channel. For bounded flows the slope of the velocity profile at the wall can be approximated by

$$b = \frac{\Delta \overline{U}}{\Delta y} = \frac{\tau_w}{\mu} \qquad (3\text{-}1)$$

where τ_w is the wall shear stress and μ is the absolute viscosity. Karpuk (1974) showed that the mean velocity profile for a two-dimensional channel flow of water is linear to about $y^+ = 6$. Here y^+ is the nondimensional distance normal to the wall defined as

$$y^+ = \frac{y u_\tau}{\nu} \qquad (3\text{-}2)$$

where u_τ is the friction velocity and ν is the kinematic viscosity. Within this linear region $\frac{\Delta \overline{U}}{\Delta y}$ is an accurate estimate of $\left.\frac{d\overline{U}}{dy}\right|_{y=0}$ and for this reason this study was conducted within the sublayer.

For the current study a micromanometer was used to sense the streamwise pressure drop across the laser anemometer test section. Since the flow is two dimensional and fully developed a force balance on the test section yields

$$\tau_w = \frac{\Delta P}{L} \frac{D_H}{4} \tag{3-3}$$

where $\frac{\Delta P}{L}$ is the streamwise pressure gradient in the test section and D_H is the hydraulic diameter. But, as the desired quantity is the shear rate defined by Equation (3-1), Equation (3-3) can be rewritten as

$$\frac{\Delta \overline{U}}{\Delta y} = \frac{1}{\mu} \frac{\Delta P}{L} \frac{D_H}{4}. \tag{3-4}$$

In micromanometer variables this becomes

$$\frac{\Delta \overline{U}}{\Delta y} = \frac{1}{\mu} \frac{\Delta h \rho g D_H (SG - 1)}{4 L g_c}. \tag{3-5}$$

Here Δh is the change in height of the manometer fluid between static (no flow) and dynamic conditions and SG is the specific gravity of the manometer fluid. Thus, it becomes a matter of making laser anemometer measurements of the mean velocity at several y locations inside the viscous sublayer ($y^+ \leq 6$) while simultaneously taking pressure drop measurements across the same test section. The slope of the velocity profile deduced from pressure drop measurements, Equation (3-5), can be directly compared to the slope of the anemometer profile generated from both the period averaged

and the frequency averaged velocity data.

The data of Karpuk (1974) show that the turbulent intensities in the viscous sublayer can be on the order of 30% or more of the local mean velocity. According to the proposed statistical biasing corrections, the amount of biasing for this flow situation should increase the estimate of mean velocity by about 10%. Clearly if biasing of the data occurs, the so-called "biased" (frequency-averaged) velocity profile should lie 10% above the "true" velocity profile deduced from pressure drop measurements. Likewise the credibility of the proposed biasing corrections is easily tested by comparing the "bias-corrected" (period-averaged) profile against the pressure drop profile. This type of comparison from independent sources has the potential to verify the existence of the biasing and to test the adequacy of the proposed corrections. Moreover, the pressure drop measurements are unaffected by the duty cycle of the LDA, thus they are also a good standard for testing the effects of duty cycle on sampling bias.

The Laser Doppler Anemometer

The laser anemometer is essentially the individual realization device employed by Karpuk (1974) and is unchanged from his arrangement except for a slightly refined traverse system and different polaroid filter settings in the receiving optics (see Appendix B). The refined traverse allows location of the anemometer probe volume to an accuracy

of ± 0.0001 inch with respect to any other y location at centerline height in the channel. Since the viscous sublayer is a thin region of very large velocity fluctuations it is necessary to utilize a laser anemometer with good spatial resolution and a large bandwidth. The large bandwidth can be achieved by removing the pedestal frequency from the Doppler signal.

In highly turbulent flows, as in the viscous sublayer, this pedestal removal cannot be accomplished by electronic filters without filtering some of the low speed velocity realizations. For these reasons, the pedestal cancelling optics with the probe volume miniaturization described by Karpuk (1974) were used in this study. Figure 1 shows the general optical configuration of the anemometer.

The effect of the probe volume miniaturization is to make the probe volume cross section thinner in the direction normal to the wall. The dimensions of the probe volume before miniaturization can be predicted according to the methods described by Brayton and Goethert (1970). The final probe volume size depends upon the amount the laser beams are expanded in the direction normal to the channel walls ahead of the final converging lens. In this case, the beam expansion was a factor of four and the sine of the beam intersection half angle was $\sin(\frac{\theta}{2}) = 0.03383$. This produced a physical probe volume at the $\frac{1}{e^2}$ points 0.3289 inch high in the vertical direction and 0.00985 inch wide in the streamwise direction. The critical dimension normal to the

channel wall after the miniaturization was 0.00246 inch. For the Spectra Physics 5mW He-Ne laser used and the half angle given, Equation (1-1) gives the probe volume fringe spacing, S, and the Doppler conversion constant $\frac{F}{U}$, as 9.35 μm and 32,598 Hz/ft/sec, respectively.

The remaining important feature of the anemometer used by Karpuk (1974) and the current study is the pedestal-cancelling optics described by Bossel, Hiller, and Meier (1972). The basic principle is to establish two fringe patterns in the probe volume displaced in space by one-half of the fringe spacing. This 180° phase shifting creates two signals 180° out of phase for every particle traversing the probe volume. When these two signals are independently detected and then subtracted, the Doppler frequency is reinforced and the pedestal frequency is eliminated. The high pass electronic filter can therefore be removed from the system and the dynamic range of the anemometer is greatly increased.

The complete laser anemometer is mounted on a 50 inch long, one inch thick piece of aluminum. This piece was then mounted through ball bearings on slide rails positioned under the channel and attached to a micrometer traverse mechanism. The dial micrometer position readout is graduated with 0.0001 inch divisions. The traverse was not connected to the channel in any way, and the complete anemometer, sending and receiving optics, was moved to change the probe volume y location in the flow. Figure 2 illustrates the overall

arrangement of the sending and receiving optics with respect to the channel.

Because the near wall region is so small, about 0.014 inch for this study, and because at least three distinct points are necessary to determine the sublayer velocity profile from the laser anemometer data, it was extremely important to be able to locate the channel wall accurately. Even with the probe volume miniaturization, only about six distinct y locations could be sampled. Here the y location of the probe volume is the distance from the probe volume center to the wall. Missing the wall location by more than a probe volume diameter would eliminate one and possibly two y locations for measuring $\overline{U}$. Likewise, the resolution of the anemometer depends on the laser beams having a clear, undisturbed path through the water to the measurement point. This was guaranteed by uniformly bowing the channel walls inward 0.050 inch with the channel running at the desired flowrate. It was then possible to slowly traverse the probe volume in and out from the channel wall until a few low velocity realizations were detected by the receiving optics. It was also possible to physically see the change in the probe volume appearance as it touched the wall. Used together, these two techniques were found to be repeatable to 0.001 inch, or approximately one-half the probe volume thickness. On several occasions it was possible to locate the wall to within 0.0003 inch. The exact wall location

was determined later by the zero intercept of the velocity profile data.

Data Acquisition and Reduction Electronics

The data reduction scheme for this study utilized a combination of the visual verification technique described by Karpuk (1974) and the recently acquired DISA 55L90 Counter Processor. However, the data acquisition electronics for both cases were the same. Figure 3 is a block diagram of the electronic signal processing as it was done during a measurement run with the laser anemometer. Two RCA photomultiplier tubes, a 7265 and 7326, with S-20 spectral response were used. They were powered by a common 2000 volt power supply and their outputs were balanced using different loading resistors. The "A-B" signal from the preamplifier of a Tektronics 502A oscilloscope was recorded on an Ampex Model 1300 magnetic tape deck at 60 inches per second. A Multimetrics Model AF120 band pass filter was used to eliminate electronic noise well outside the expected Doppler frequency bandwidth.

For visual verification the data was replayed at 7½ inches per second into the electronic arrangement shown in Figure 3. The Schmitt trigger converts each Doppler burst into a pulse train which simultaneously triggers the General Radio 1192B counter operating in the period times ten mode and a Tektronics 564B storage oscilloscope. The counter

output displayed on the storage oscilloscope is visually verified to contain at least ten evenly spaced, consecutive pulses, the number averaged by the counter. All verified counts were punched on a Tally Model P-120 paper tape punch connected to the BCD output of the General Radio counter through an NLS Serializer. This paper tape record of Doppler periods was then read into a Hewlett Packard 9820 computer which processed the data to yield period averaged and frequency averaged mean velocity, the corresponding turbulent quantities, and the random error in the mean velocity at the 95% confidence level. The computer program also provides a histogram of the uncorrected, "biased", velocity realizations.

The other type of data reduction used the DISA 55L90 LDA Counter Processor. The 55L90 Processor replaced the manual operator visually verifying data and allowed real-time (60 IPS) replay of the recorded Doppler signals. (For a detailed description of the 55L90 Processor operation, see Appendix A.) Figure 3 shows a block diagram of the equipment arrangement for using the 55L90 Processor. The signals from the magnetic tape are first passed through the Multimetrics band pass filter as during the actual anemometer run to eliminate electronic noise. An external attenuator was used before the signals entered the 55L90 Processor so that the approximately 2-3 volt peak-to-peak amplitude signals recorded on magnetic tape could be reduced to the 2 volt limit of the 55L90. The digital output of the counter

module is a form of binary code containing the frequency of the Doppler signal, F. This frequency output is in the form

$$D = D_m \times 2^E \qquad (3\text{-}6)$$

where D_m is an eight bit binary mantissa and E is a four bit binary exponent. This number is converted into the Doppler frequency, F, of the taped input signal through the algorithm

$$F = \frac{D \times N_H \times 10^9}{32640 \times 2^{15}} H_z \qquad (3\text{-}7)$$

where N_H is eight for the 55L90 used in this study (see Appendix A).

An integrated circuit interface converted the binary output of the 55L90 Processor to a decimal (ten level) code acceptable to the NLS Serializer. The output was finally punched on paper tape with a Tally Model P-120 paper tape punch. The HP 9820 program for calculating the mean and turbulent velocity information from the DISA counter output is basically the same as before. The main difference is that the program must first convert the DISA mantissa-plus-exponent format to a frequency.

Pressure Drop Measurements

Pressure drop measurements were made with a micrometer type two-fluid manometer. This micromanometer can sense water pressure changes of +0.0005 inch. The indicating

fluid used in this study was carbon tetrachloride, CCl_4, with a specific gravity, SG = 1.58224 with respect to water at 25°C. The specific gravity was determined to ±0.1% using a 50 ± 0.05 ml volumetric flask and a Mettler precision balance accurate to ±0.00001 gram.

The pressure taps, Figure 4b were located at either end of the channel test section on the centerline as shown in Figure 4a. The taps were spaced 18.0 inches apart, and the downstream tap was located about six channel widths upstream of the channel exit. The two identical pressure taps were designed and constructed according to the criteria described by Shaw (1959). Figure 4b shows a cross section of the design. Since both taps exhibit the same pressure hole error (see Shaw, 1959) the pressure difference across them, the quantity being measured, does not exhibit any error due to the hole configuration but only the errors due to reading the manometer. This system of pressure taps, micromanometer, and CCl_4 was certified to give a reasonable value of pressure drop for the range of flow rates used in this study by comparison with standard friction factor curves. One such comparison is shown in Figure 5.

Flow Channel and Seeding

All flow measurements were made in the two-dimensional water channel described in detail by Reischman (1973) and Karpuk (1974). The only modifications made on the channel were to the downstream wier tank and the addition of

centerline pressure taps at the test section. Because of the need for highly accurate pressure drop measurements it was desirable to generate a flow that would maintain a constant, steady head over extended periods of time. A good method of accomplishing this is to make the wier tank as large as possible. Another technique is to introduce baffles and screens into the flow to make it more uniform.

The wier tank, Figure 6, was completely rebuilt on a larger scale than before and screens were added to help redistribute and diffuse the flow exiting the channel. The screens so successfully damped out the flow oscillations and broke up the jet coming from the channel that the height of the water flowing over the wier was essentially constant ($\pm$0.020 inch) for a given flow rate. The clear acrylic channel is 72 inches long, 12 inches high, and 1.018 inch wide at the centerline. The vertical walls were bowed inward 0.050 inch along the channel length while the channel was running at the desired flow rate. As mentioned earlier, this bowing allowed the anemometer probe volume to be traversed up to the wall without interference. Measurements were made 55 channel widths downstream of a sharp-edged Borda type entrance. Figure 6 is an overall view of the all stainless steel and plastic facility.

The flow of water is produced by a 200 GPM pump which continuously recirculates the make up water. This make up water, normally 250 gallons, was filtered through 0.5 μm filters before passing into the flow loop. It was then

carefully seeded with a measured amount of 5-10 μm certified AC Fine Test Dust. This size particle was shown by Reischman and Tiederman (1973) using the criteria of Hjelmfelt and Mockros (1965) to accurately follow the range of flow oscillations encountered in this study. The optimum particle size for good Doppler signals using the anemometer described above is approximately 5 μm in diameter (see Durst and Whitelaw, 1972).

Corrections Applied to the Data

The corrections applied to the data are those described by Karpuk (1974). Besides the McLaughlin-Tiederman biasing correction to remove the affects of statistical biasing, a correction was applied to account for the effect of a finite sized probe volume on the mean velocity and the turbulent quantities. This was required since the near wall region has a strong velocity gradient which can create a significant change in mean velocity and fluctuating velocity across the finite sized probe volume. It has been suggested* that a correct form of the RMS velocity fluctuation at the center of the probe volume, u_o', is

$$u_o' = \left[\frac{u_m'^2 - \frac{s_w^2}{12}}{\left(1 + \frac{s_w^2}{12\overline{U}^2}\right)}\right]^{1/2}. \qquad (3\text{-}8)$$

Here u_m' is the RMS velocity fluctuation from period

*M. E. Karpuk, and W. G. Tiederman, submitted to AIAA Journal (1975).

averaged data.

s is the slope of the sublayer velocity profile.

w is the width of the probe volume.

$\overline{U}$ is the period averaged mean velocity.

The mean velocity is corrected for finite probe volume effects using the McLaughlin-Tiederman statistical biasing correction (see Karpuk, 1974).

CHAPTER IV

EXPERIMENTAL RESULTS

The laser anemometer and micromanometer were successfully used to independently measure the wall slope of the velocity profile in a fully developed, turbulent flow of water. The two dimensional channel measurements were made at four values of Reynolds numbers from Re = 14,011 to Re = 17,959 where $Re = \frac{\overline{U}_a D_H}{\nu}$. A comparison of the two kinds of profiles demonstrates that statistical biasing as proposed by McLaughlin and Tiederman (1973) does exist and creates a significant error in the estimate of the mean and fluctuating velocity components. The comparison of mean velocities measured for various seed densities in a given flow indicate that the statistical biasing is independent of seed density over the range of duty cycles encountered here.

Statistical Biasing

Four data runs were made over a Reynolds number range based on hydraulic diameter, D_H, and mass average velocity, $\overline{U}_a$, of 14,011 to 17,959. Table I shows the three runs used to compare pressure drop to laser anemometer data and a fourth run, BC-2, which was used to look at single point seed density effects discussed later. A typical velocity profile

showing the wall location by the zero velocity intercept is illustrated in Figure 7 containing both the frequency averaged and period averaged velocity profiles. All subsequent figures will be shifted so that the y = 0 location corresponds to the zero velocity intercept. This was done because the accuracy in locating each point with respect to the others was much greater than the accuracy in locating the wall. The amount of shift ranged from 0.0005 inch for BC-5.2 to 0.0015 for BC-6. The BC-3 zero velocity intercept was shifted 0.0008 inch.

The results of the laser anemometer measurements are presented in Table II. The $\overline{U}_c$ values have been corrected for both statistical biasing and finite probe volume effects described earlier. The y values are the shifted y locations and except for BC-2 the y^+ values are all based on the shear velocity calculated from the pressure drop measurements. The shear velocity for BC-2 is based on the slope of the mean velocity profile. The fifth column to the right of the run number, $\frac{\overline{U}_e - \overline{U}_c}{\overline{U}_c} \times 100$, is the percentage difference between the period average and frequency average mean velocity. Likewise the second to last column, $\frac{(u' - u'_o)}{u'_o} \times 100$, is the percentage difference between the RMS fluctuation estimated from $u' = \frac{1}{N-1} \Sigma (U_i - \overline{U})^2$ and the fluctuation corrected for sampling bias and finite probe volume effects, u'_o.

These results are compared to the linear profile deduced from the pressure drop measurements in Figure 8

through Figure 10. The lines through the anemometer data points are the least squares fit of the four data points and, unless otherwise illustrated, the 95% confidence limits are the same size as the mark identifying the point. The pressure drop profiles are represented as bands instead of single lines to represent the upper and lower limits for the ΔP measurement. Any systematic errors in using the anemometer and electronic processing equipment were estimated to be less than one percent.

For the data in Figures 8, 9, and 10, the period average mean velocity profile agrees reasonably well with the pressure drop profile while the frequency average mean velocity profile shows poor agreement. Figure 8 graphically illustrates a problem encountered in making accurate pressure drop measurements for all of the data runs. In each case, the manometer reference height (zero flow) value measured prior to the run differed from the value measured after the run. For BC-3, this "zero" shift created a large amount of uncertainty in the pressure drop measurement. These three data runs are plotted nondimensionally in law of the wall coordinates, U^+ vs y^+, in Figure 11. The mean velocity, $\overline{U}$, was nondimensionalized with the friction velocity, u_τ. Here $u_\tau = (\frac{\tau_w}{\rho})^{1/2}$ where τ_w was deduced from the pressure drop measurements. The nondimensional y coordinate was determined from $y^+ = \frac{yu_\tau}{\nu}$ where ν is the kinematic viscosity. This figure plainly demonstrates the effect of biasing on the mean velocity profile for low duty cycle individual

realization anemometer measurements. The period average data, corrected with the one dimensional biasing correction suggested by McLaughlin and Tiederman (1973), lie along the $U^+ = y^+$ line while the frequency average (biased) data lie substantially above the $U^+ = y^+$ line. Since $U^+ = y^+$ for the viscous sublayer, Figure 11 demonstrates that the period average velocity approximates the "true" velocity.

A numerical comparison of the slope of the anemometer profiles with the slope deduced from pressure drop measurements is shown in Table III. For the anemometer data, the mean value of slope was calculated using a least squares regression of the four data points for each run shown in Table II. The y values used in the regression were not shifted for the $y = 0$ intercept. An analysis of the variance to determine the 95% confidence limits of the uncertainty in the mean anemometer slope values, based only on the four data points for each case, produced unrealistically large uncertainty bands. A better estimate of the mean value of the slope and the uncertainty of the estimate is determined from a least squares regression of all of the individual velocity realizations for a data run. Such a technique cannot be applied to the period average data but is easily used with the frequency average velocity realizations directly from the computer output. The regression of all the velocity realizations compares favorably with the regression of only the four data points (mean velocities) for the frequency average data. Thus, a least squares regression of

the four period average mean velocities of each run gives a reasonable value for the slope of the bias-corrected mean velocity profile.

The 95% confidence intervals on the uncertainties in the slope of the period average velocity data were estimated from the analysis of the variance of all of the velocity realizations for the frequency average from the corresponding data run. This is a reasonable procedure since the "biased" and "bias-corrected" velocities are from the same ensemble of velocity realizations and the uncertainties should be of the same magnitude. This can be demonstrated by considering the root mean square uncertainty of the anemometer slopes based on the uncertainty in $\Delta\overline{U}$ and Δy from the relationship $b = \frac{\Delta\overline{U}}{\Delta y}$. Here $\Delta\overline{U}$ and Δy are the difference in $\overline{U}$ and y for the two most widely separated values for each data run. Such a comparison shows the validity of estimating the uncertainties of the period average slopes from the frequency average data.

Table III shows the mean value of the slope of the velocity profile calculated from four data points for each run. It also shows the mean slope calculated from all of the frequency average velocity realizations for each case (the second value for $\overline{U}_e$) and the pressure drop measurement.

The uncertainty estimates on the value of the slope of the velocity profile calculated from pressure drop measurements are calculated from the square root of the sum of the squares of the uncertainties on the components of Equation

(3-5). The principle source of error for these measurements is an accurate determination of Δh, the change in height of the manometer fluid. The zero position of h (no flow) for each run changed slightly between prerun and post-run static conditions. This zero shift accounted for most of the ΔP error and ranged from less than 1% of Δh for BC-5.2 to about 8.7% of Δh for BC-3. The total of the uncertainties of the rest of Equation (3-5) was always about 1%. Systematic errors are assumed to be small enough as to be negligible.

A statistical comparison of the slopes of the anemometer and pressure drop measurements in Table III was not made since no adequate test was found to compare mean slope values from two different sample populations. However, if the slope computed from the pressure drop measurements is assumed to be the exact value of the slope of the velocity profile it is a simple matter to show that the period average slope is statistically the same as the pressure measurement for each case. It is also evident that the frequency average slope is not the same as the pressure measurement for each data run.

The only other method of comparing the slopes is to show that the uncertainty bands of the pressure drop measurement overlap the uncertainty bands for the period average data, but do not overlap for the frequency average data. The former is true for every data run, and the latter is true for BC-5.2. The uncertainty bands for the pressure drop measurement and frequency average velocity data just

coincide at their extreme upper limit and lower limit, respectively, in BC-3. For BC-6 the "biased" velocity profile slope overlaps the pressure drop measurement band about 3%. Such overlap is not significant and the probability that the "biased" data represents the pressure drop data is small.

Another comparison of period average and frequency average data reductions is shown in Figure 12. The figure illustrates the relative difference between the "biased" (frequency average) and "corrected" (period average) mean velocities as a function of turbulent intensity. The theoretical curves were calculated according to the biasing correction techniques proposed by McLaughlin and Tiederman (1973). The curves are the relative error between the biased and corrected mean velocities for both a one dimensional correction and a two dimensional correction to a modified Gaussian distribution of velocities with $\frac{v'}{u'} = 0.5$ and $R_{12} = -1$. Here R_{12} is the correlation coefficient, $\frac{\overline{uv}}{u'v'}$.

The turbulent intensities for the three data runs are plotted in two different ways in Figure 13 and Figure 14. Figure 13 is $\frac{u'_o}{u_\tau}$ plotted against y^+. As before, $y^+ = \frac{yu_\tau}{\nu}$ where u_τ was derived from the pressure drop data. It should be noted that the data from the current study agree quite well with data from Hussain and Reynolds (1975). The unweighted average turbulent intensity and the weighted average turbulent intensity corrected for finite probe

volume effects are plotted against y^+ with data from Karpuk (1974) in Figure 14. The data from the present study correspond closely to his results despite the different methods of computing y^+. This result substantiates the Karpuk and Tiederman correction for finite probe volume effects shown in Equation (3-8).

Seed Density Effects

The effect of seed density on the statistical biasing of the mean velocity was not adequately investigated by this experimental work. Despite varying the seed density over a fairly wide range the duty cycle of realizations was always less than 4%. This means that seed particles were in the probe volume only about 4% of the run time or less. Since the important criteria for judging seed density effects is not the physical concentration of seed particles in the flow, but the duty cycle, the data contained in Table IV simply demonstrates the effect of seed density in a small range of duty cycle. For the data runs presented the two values of seed density in each case are for the same y location in the same flow. The seed density is given in terms of grams of AC Test Dust per 250 gallons of makeup water. As suggested by McLaughlin and Tiederman (1973) there is no measurable effect on the mean velocity for these variations in seed density.

The significance of the low duty cycle, low seed density flows presented in this study is that statistical

biasing clearly occurs and can often create a significant error in estimating the mean velocity and the fluctuating quantities. According to Barnett and Bentley (1974), statistical biasing of individual realization data should not occur for low values of duty cycle such as encountered in this study. However, the data presented here do not support such a conclusion and appear to verify the existence of statistical biasing.

CHAPTER V

SUMMARY AND CONCLUSIONS

An individual realization laser anemometer and a pressure sensing micromanometer were simultaneously used to independently determine the slope of the mean velocity profile in the viscous sublayer of a two-dimensional, turbulent channel flow of water. The one-dimensional statistical biasing correction for individual realization laser anemometer data proposed by McLaughlin and Tiederman (1973) was applied to the laser anemometer data. The frequency average and period average mean velocities were then compared to the velocity profile deduced from the pressure drop measurements. In conjunction, several different concentrations of scattering particles were used to determine the effects of seed density upon the statistical biasing for a range of low duty cycles.

The conclusions drawn from this study are that:

(1) Statistical biasing of the mean velocity computed from a simple ensemble average or frequency average of the individual velocity realizations does occur.

(2) A reasonably accurate estimate of $\overline{U}$ is given by the one-dimensional correction where each

individual velocity realization in the ensemble is weighted with the inverse of the instantaneous streamwise velocity.

(3) The amount of the correction can be as much as 10% for turbulent intensities greater than 30%.

(4) Statistical biasing is unaffected by variations in the concentration of light scattering particles for duty cycles between 1.3% and 3.4%.

SELECTED BIBLIOGRAPHY

Barnett, D. O., and H. T. Bentley, III.

1974 "Statistical Bias of Individual Realization Laser Velocimeters." Proceedings of the Second International Worshop on Laser Velocimeters, Vol. I. West Lafayette, Indiana: Purdue University, pp. 428-442.

Bossel, H. H., W. J. Hiller, and G. E. A. Meier.

1972 "Noise Cancelling Signal Difference Method for Optical Velocity Measurements." J. Physics, E., J. Sci. Instr., Vol. 5, pp. 893-896.

Brayton, D. B., and W. H. Goethert.

1970 "A New Dual-scatter Laser Doppler-shift Velocity Measuring Technique." ISA Trans., Vol. 10, No. 1, pp. 40-50.

Donohue, G. L., D. K. McLaughlin, and W. G. Tiederman.

1972 "Turbulence Measurements With a Laser Anemometer Measuring Individual Realizations." Phys. of Fluids, Vol. 15, pp. 1920-1926.

Draper, N. R., and H. Smith.

1968 Applied Regression Analysis. New York: John Wiley and Sons, Inc.

Durst, F., and J. H. Whitelaw.

1972 "Theoretical Consideration of Significance to the Design of Optical Anemometers." ASME Paper No. 72-HT-7. Denver, Colorado: Heat Transfer Conference.

Hjelmfelt, A. T., and L. F. Mockros.

1965 "Motion of Discrete Particles in a Turbulent Field." Appl. Sci. Res., 16, p. 149.

Hussain, A. K. M. F., and W. C. Reynolds.

1975 "Measurements in Fully Developed Turbulent Channel Flow." ASME Paper No. 75-FE-5. Minneapolis, Minnesota: Fluids Engineering Conference.

Karpuk, M. E.

1974 "A Laser Anemometer for Viscous Sublayer Measurements." (Unpub. M. S. Thesis, Oklahoma State University.)

McLaughlin, D. K., and W. G. Tiederman.

1973 "Biasing Correction for Individual Realization Laser Anemometer Measurements in Turbulent Flows." Phys. of Fluids, Vol. 16, No. 12, pp. 2082-2088.

Reischmann, M. M., and W. G. Tiederman.

1975 "Laser Doppler Anemometer Measurements in Drag-Reducing Channel Flows." J. Fluid Mechanics, Vol. 70, Part 2, pp. 369-392.

Salsman, L. N., W. R. Adcox, and D. K. McLaughlin.

1974 "An Evaluation of a Sequential Phase Comparison Data Processor for Laser Anemometry." Proceedings of the Second International Workshop on Laser Velocimeters, Vol. I. West Lafayette, Indiana: Purdue University, pp. 256-268.

Shaw, R.

1959 "The Influence of Hole Dimensions on Static Pressure Measurements." Department of Mechanical Engineering. Liverpool: University of Liverpool.

Tiederman, W. G., D. K. McLaughlin, and M. M. Reischman.

1973 "Individual Realization Laser-Doppler Technique Applied to Turbulent Channel Flow." Proceedings. Rolla, Missouri: The Symposium on Turbulence in Liquids, p. 172.

APPENDIX A

THE DISA 55L90 LDA COUNTER PROCESSOR

The DISA 55L90 Counter is a relatively newly-developed LDA data processor for individual realization laser anemometer measurements. The counter used here was a fully equipped model containing: (1) A High Voltage Power Supply for use with photomultiplier tubes; (2) Data Rate Module; (3) D/A Converter; (4) Mean Velocity Computer that displays either the average Doppler frequency or the period averaged mean velocity; (5) Counter Module (Comparator) that verifies incoming data and routes the good data to external system components. This appendix will give a brief description of the operating principles and procedures followed in the use of the 55L90 Processor employed in this study.

Basic Principles of Internal Operation

The incoming Doppler signal is first amplified 60 dB and then attenuated by a manually adjustable attenuator to a maximum of -31 dB. Bandpass filtering occurs before the internal Schmitt trigger converts the Doppler burst information into a pulse train. The pulse train is applied to the 5/8 fringe counter, a shift register, which begins accumulating 250 MHz clock pulses when cleared. After the low count register accumulates $N = 5$ fringe counts it stops counting and holds the low count at a value of C_L. Similarly, the high count register stops counting when $N = 8$ and holds the high count at a value C_H. Simultaneous with the closing of the AND Gate controlling the high count shift register is the "compare" command which also initiates a

command to clear the registers for the next Doppler pulse. The function of the comparator is to perform the operation

$$100 \times \left| C_H - \frac{8}{5} C_L \right| \leq e\, C_H. \qquad \text{(A-1)}$$

Here e is the percent tolerance in the outcome as set externally on the Counter Module. If the data is valid, the number existing on the comparator is changed to the new number and the comparator outputs a "data ready" command to the Computer Module or to the externally connected equipment (a Tally P-120 paper tape punch in this case). The 55L90 Processor has the additional feature of a Threshold Window built into the Counter Module. This manually adjusted device can be used to place an upper limit on the signal amplitude the Counter will accept. The purpose is to eliminate the high amplitude signals from the particles too large to accurately follow the fluid flow.

The Computer Module is designed to output either the average Doppler frequency or period averaged velocity calculated from ensembles of individual realizations. The period averaging is carried out for ensemble widths of 1, 16, 256, and 4096, and the result is appropriately scaled for the desired readout on a five digit LED display. The output is a three digit mantissa and a 2 digit power of ten.

The other important piece of equipment attached to the 55L90 Processor is the Data Rate module which displays the data validation rate in Hz, KHz, or percent.

The High Voltage Power Supply was not used during this

study and the D/A Converter was only used briefly during the preliminary evaluation of the Comparator performance.

Operational Checkout

Upon initial receipt of the 55L90 Processor the interface to link the unit to the Tally Punch was not yet completed. Therefore, the first step was to evaluate the counter with sine waves from a test oscillator. The input signals were varied across the 1000 Hz to 100 MHz range of the instrument and in amplitude from below 200mV to above 3V peak to peak to test the attenuation, Schmitt trigger levels, and the Threshold Window.

The attenuators worked as expected. The Schmitt trigger level was about 110-120 mV instead of the design level of 100 mV, however this difference was no factor in the subsequent data reduction. The last item checked with the oscillator was the Threshold Window. It was discovered that the 2 Volt maximum signal strength usable in the Counter corresponded to the 20 dB (out of 31 dB possible) setting on the Threshold Window. This 2 Volt maximum is set by the saturation limit of the Counter amplifiers. Thus, any signal of greater amplitude than 2 Volts peak to peak into the Counter will come out of the amplifiers at about 2 Volts peak to peak and sometimes slightly distorted. Therefore, all Doppler signals will pass any Threshold setting above 20 dB, but may be somewhat distorted.

The next step in the evaluation process was to set up

the electronics as shown in Figure 3 without the Tally Punch. The bandpass filter was added to compensate for the relatively wide bandwidth of the internal filter. A laser anemometer data tape from past work by Reischman (1973) was replayed into the data reduction system. The attenuation levels, ensemble widths, and the percent Comparator accuracy were varied in a number of ways and the Computer Module readout for each case was recorded. In addition, the D/A analog signal was monitored to see if the Comparator would pass signals of very low frequency that probably are not valid. In each test case, it was determined that the attenuation levels must be enough to lower the average noise level on the magnetic tape below the 110-120 mV Schmitt trigger level. For Comparator accuracies less than 12%, about two in every thousand Doppler signals verified as good signals by the Comparator were unusually low frequency although still above the high pass filter setting.

The consequence is that the mean velocity of the ensemble containing such points is abnormally low due to the period averaging done by the Computer. When the ensembles containing these signals were eliminated from the mean velocity calculations the results were repeatable and agreed favorably with data reduction done earlier by visual verification and with the Sequential Phase Comparator described by Salsman (1974). When the interfacing to convert the binary 55L90 output into the decimal output required by the NLS Serializer was ready, the electronics were set up as shown

in Figure 3. The same data tape was played into the system and the paper-taped results were reduced on the HP 9820 computer. The computer program (Chapter III) assigns arbitrary frequency limits to the results corresponding to the band pass filter settings of the data acquisition and reduction electronics. These frequency limits effectively remove the spurious low or very high frequencies from the velocity calculations if the noise levels on the magnetic tape are attenuated below the Schmitt trigger level of the 55L90 Processor. This restraint appears necessary as the results from the 55L90 seem to be sensitive to the relative position of the noise level with respect to the internal Schmitt trigger level. For this study the best results were obtained when the average noise level was well below the 110-120 mV Schmitt trigger level and the Comparator accuracy was set on 1.5 or 3.0%. Not only did the validation rate increase with lowered noise level but the mean velocities compared more favorably with past measurements. The results of these tests demonstrated that the data reduced on the DISA 55L90 Processor was in reasonable agreement with past data reductions by other methods.

Additional Comments

Because the DISA 55L90 Processor reset time is so short (about 100 nsec), all data can be replayed at real time (60 IPS) during reduction. In this case, the Tally P-120 paper tape punch was the limiting factor in the speed of

data reduction since it required approximately 50 msec to punch a five-digit number. For the particular laser anemometer and data reduction used, the 1000 Hz lower limit on the Counter Module high pass filter put a serious restriction on the slowest velocities that could be measured. Hence, the first y location to be sampled in the channel was carefully chosen to guarantee that all Doppler frequencies would be greater than 1000 Hz. This particular "problem" could easily be solved by changing the anemometer sending optics or by recording at a tape speed lower than 60 IPS and replaying the tape at 60 IPS.

The maximum Threshold setting was used for all of the data reduced on the 55L90 Processor during this study. This was possible because the seed particles were all within a given size range known to accurately follow the flow. The Comparator accuracy was arbitrarily set at 3% which gave results comparable to the 1.5% setting but a much larger number of data points.

APPENDIX B

PEDESTAL CANCELLING OPTICS

The pedestal cancelling optics described in the section "The Laser Doppler Anemometer" operate on the same principle as those described by Bossel, Hiller, and Meier (1972) and Karpuk (1974) but the polarizations used in the receiving optics were quite different for this study. For the particular beam splitter used in the receiving optics it was impossible to get good pedestal cancellation by setting the two polaroid filters at $\pm 45^{\circ}$, respectively. The cause of the difficulty was the preferred angle of polarization for the beam splitter used here which was not $\pm 45^{\circ}$ but 135°. That is, the maximum amplitude signal from the photomultiplier occurred when both polaroid filters were set on 135°. This was also the best setting for pedestal cancelling.

This particular arrangement was discovered by measuring the amplitude of a laser beam exiting the beam splitter for a range of incoming beam polarizations between 0° and 180°. The maximum output signal occurred when the polaroid filter was set either at 45° or 135°. This was true for both exit faces of the beam splitter. Obviously there were six possible combinations of polarization settings for the two filters in front of the photomultiplier tubes. However, the only combination that gave good pedestal cancelling and large amplitude signals was $+135^{\circ}$ for both polaroids and not the $\pm 45^{\circ}$ described by previous experimenters.

APPENDIX C

DATA

TABLE I

DATA RUN PARAMETERS - AVERAGE VALUES

Run #	R_e	$\dot{Q}$(GPM)	$\overline{U}_a$(ft/sec)	T($^\circ$C)	Manometer Δh (in)
BC-2	14,011	31	0.7762	28	
BC-3	17,504	37	0.9264	29	0.0686
BC-5.2	17,959	37	0.9264	31	0.0599
BC-6	14,838	29.5	0.7386	33	0.0410

TABLE II

LASER ANEMOMETER RESULTS

Run # % Duty Cyc.	y (in)	y^+	$\bar{U}_c$ (ft/sec)	$\bar{U}_e$ (ft/sec)	$\frac{\bar{U}_e - \bar{U}_c}{\bar{U}_c} \times 100$	u_o' (ft/sec)	u' (ft/sec)	$\frac{\bar{u} - u_o'}{u_o'} \times 100$	N
BC-2	.00325	1.36	.0593	.0677	14.2	.0223	.0302	35	310
	.0049	2.05	.0999	.1114	11.5	.0308	.0352	14	509
	.0119	4.98	.2230	.2508	12.5	.0774	.0823	6.3	371
BC-3	.00469	2.40	.1251	.1430	14.3	.0426	.0536	25.8	1748
	.00579	2.96	.1595	.1802	13.0	.0537	.0601	11.8	2162
2.22-3.35	.00929	4.76	.2523	.2865	13.6	.0906	.0979	8.1	1571
	.01059	5.42	.2868	.3254	13.5	.1032	.1088	5.5	1658
BC-5.2	.00719	3.60	.1728	.1992	15.3	.0648	.0727	12.9	1465
	.00824	4.12	.2028	.2331	14.9	.0760	.0866	14.0	1114
1.66-2.90	.01104	5.52	.2739	.3154	15.2	.1049	.1127	7.4	1310
	.01214	6.07	.2970	.3377	13.7	.1083	.1180	9.0	1332
BC-6	.0100	4.28	.1774	.2035	14.7	.0668	.0736	10.2	1479
	.0111	4.75	.2016	.2303	14.2	.0749	.0827	10.4	1323
1.34-2.52	.0129	5.52	.2311	.2622	13.5	.0838	.0904	7.9	1350
	.0139	5.95	.2446	.2791	14.1	.0909	.0970	6.8	1084

TABLE III

PROFILE SLOPES

Run #		BC-3	BC-5.2	BC-6
$b = \frac{\Delta \overline{U}}{\Delta y}$ $\left(\frac{ft}{sec\ in}\right)$	ΔP	27.60 ±8.8%	25.19 ±2.10%	17.84 ±5.59%
	$\overline{U}_c$	27.16 ±2.7%	25.16 ±2.2%	17.11 ±5.24%
	$\overline{U}_e$ 1.	30.77	27.40	19.11
	2.	30.73	28.34	19.28
		±2.57%	±2.12%	±4.98%

TABLE IV

SEED DENSITY EFFECTS

Run #	y (in)	y^+	ρ_s ($\frac{gm}{250\ gal}$)	% Duty Cycle	$\overline{U}_c$ (ft/sec)	$\pm Err_c$	$\overline{U}_e$ (ft/sec)	$\pm Err_e$	u_o' (ft/sec)	$\frac{u_o'}{\overline{U}_c}$
BC-2	.0119	4.98	2	NA	.2187	.0042	.2507	.0044	.0825	.3772
			½		.2191	.0045	.2645	.0046	.0986	.4502
BC-3	.01059	5.42	2	2.22	.2868	.0051	.3254	.0052	.1032	.3597
			½	0.68	.2988	.0044	.3347	.0045	.1015	.3397

APPENDIX D

FIGURES

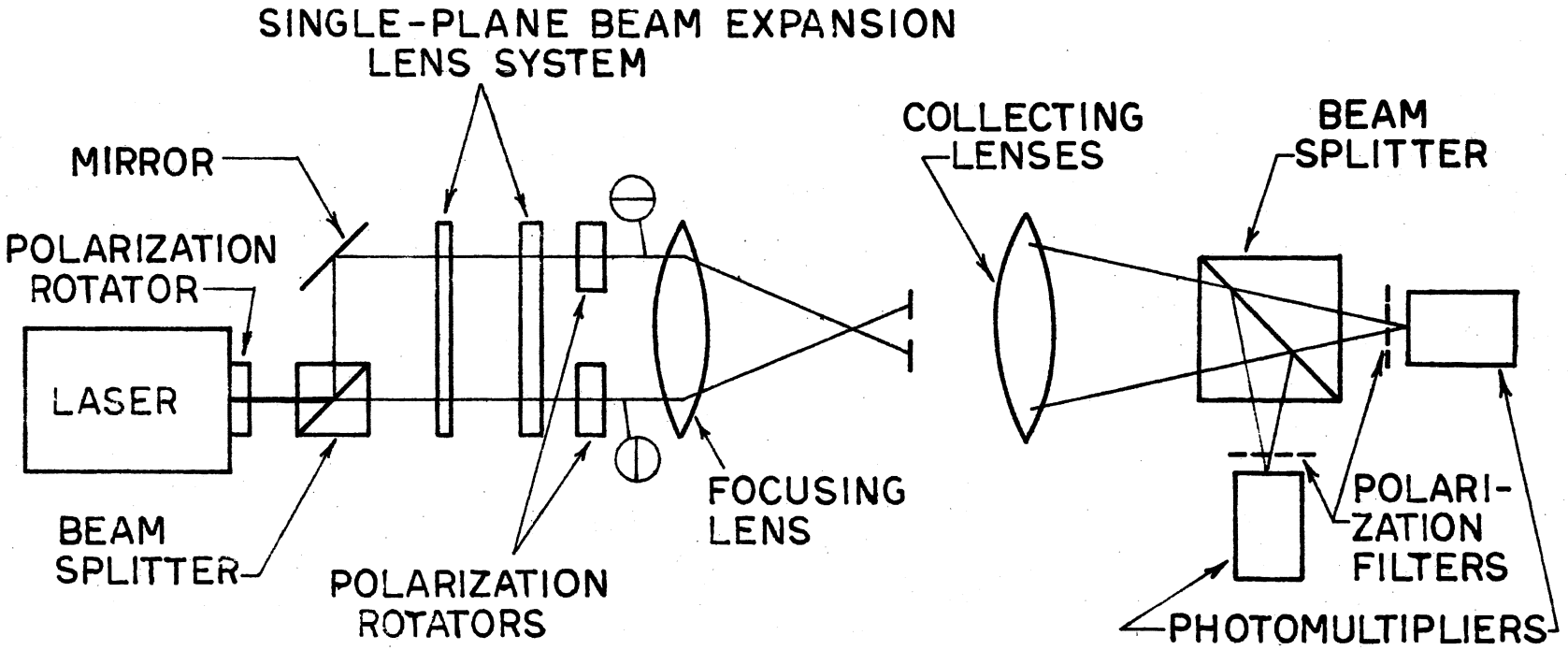

Figure 1. Schematic of the Optical System

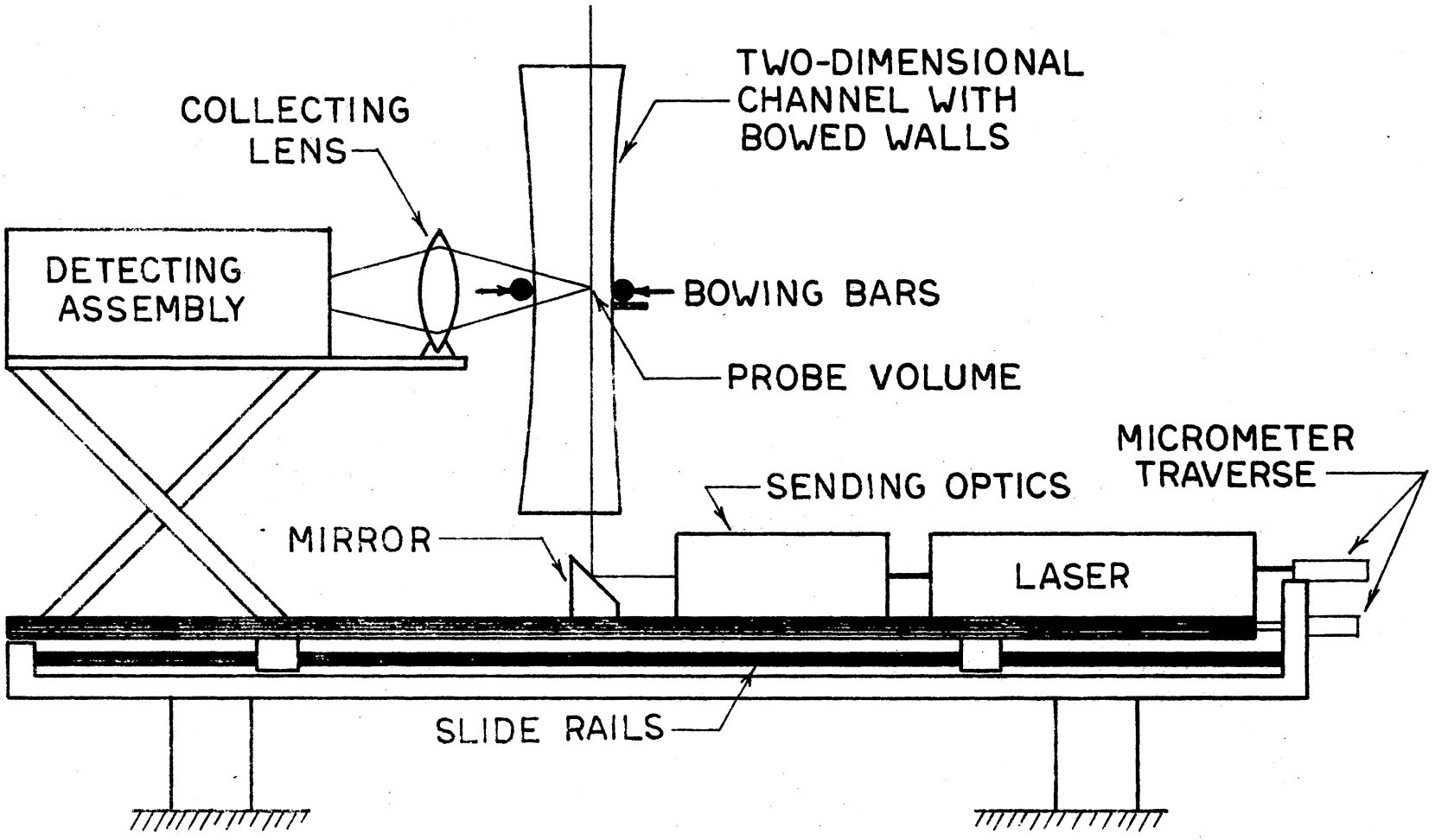

Figure 2. Schematic of the Flow Channel and the Anemometer

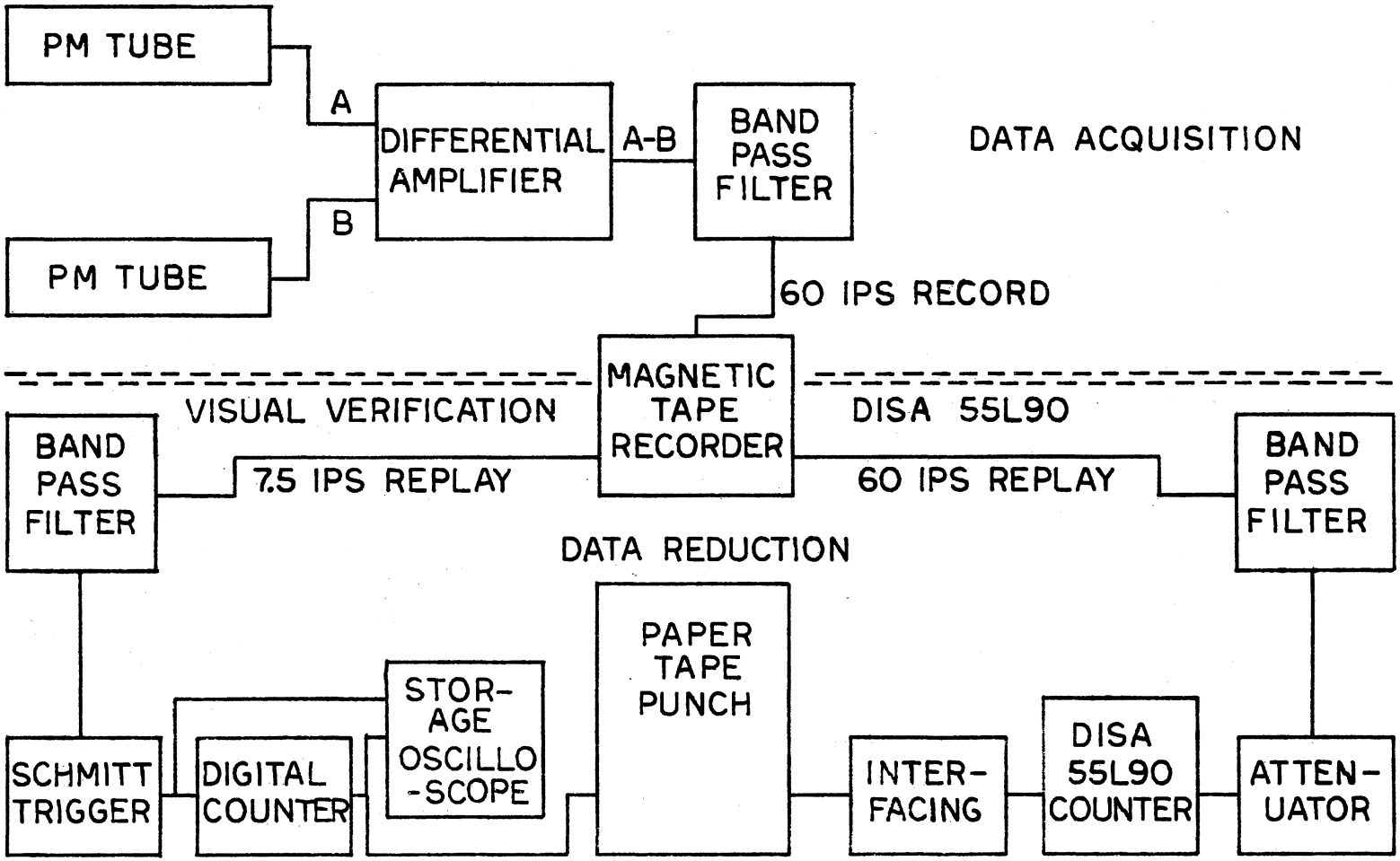

Figure 3. Block Diagram of Data Acquisition and Reduction Electronics

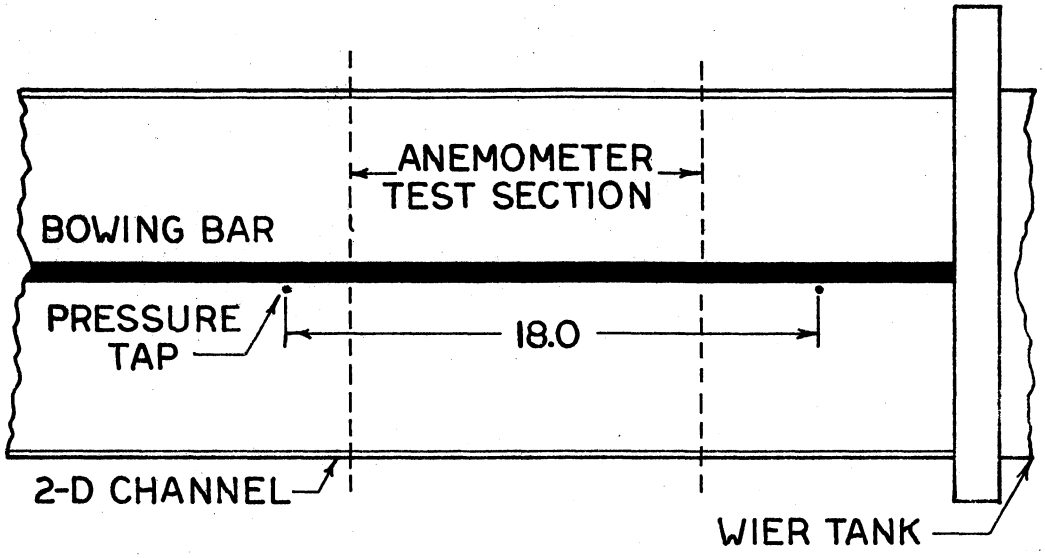

(a) Pressure Tap Location

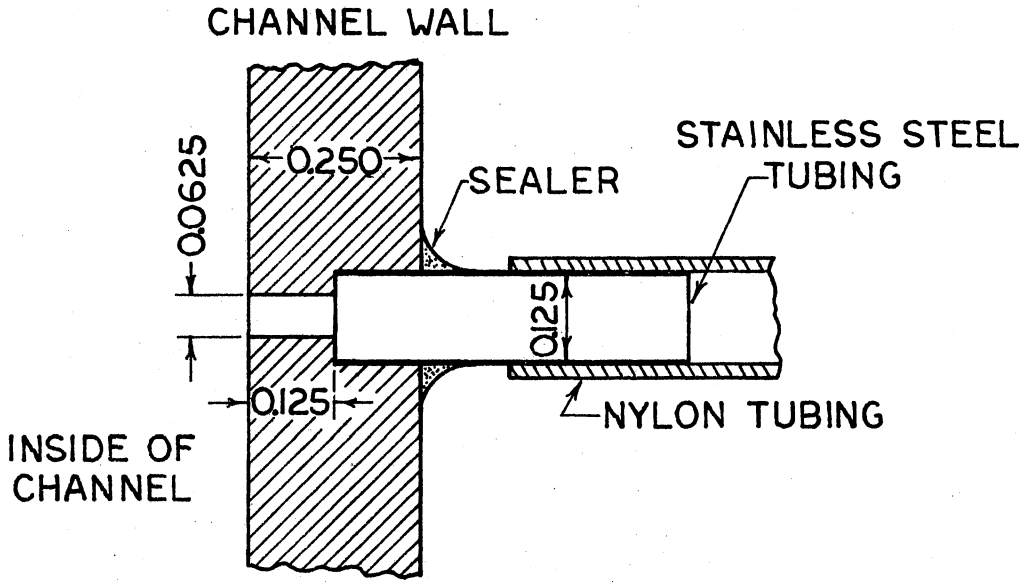

(b) Pressure Tap Cross Section

Figure 4. Pressure Taps

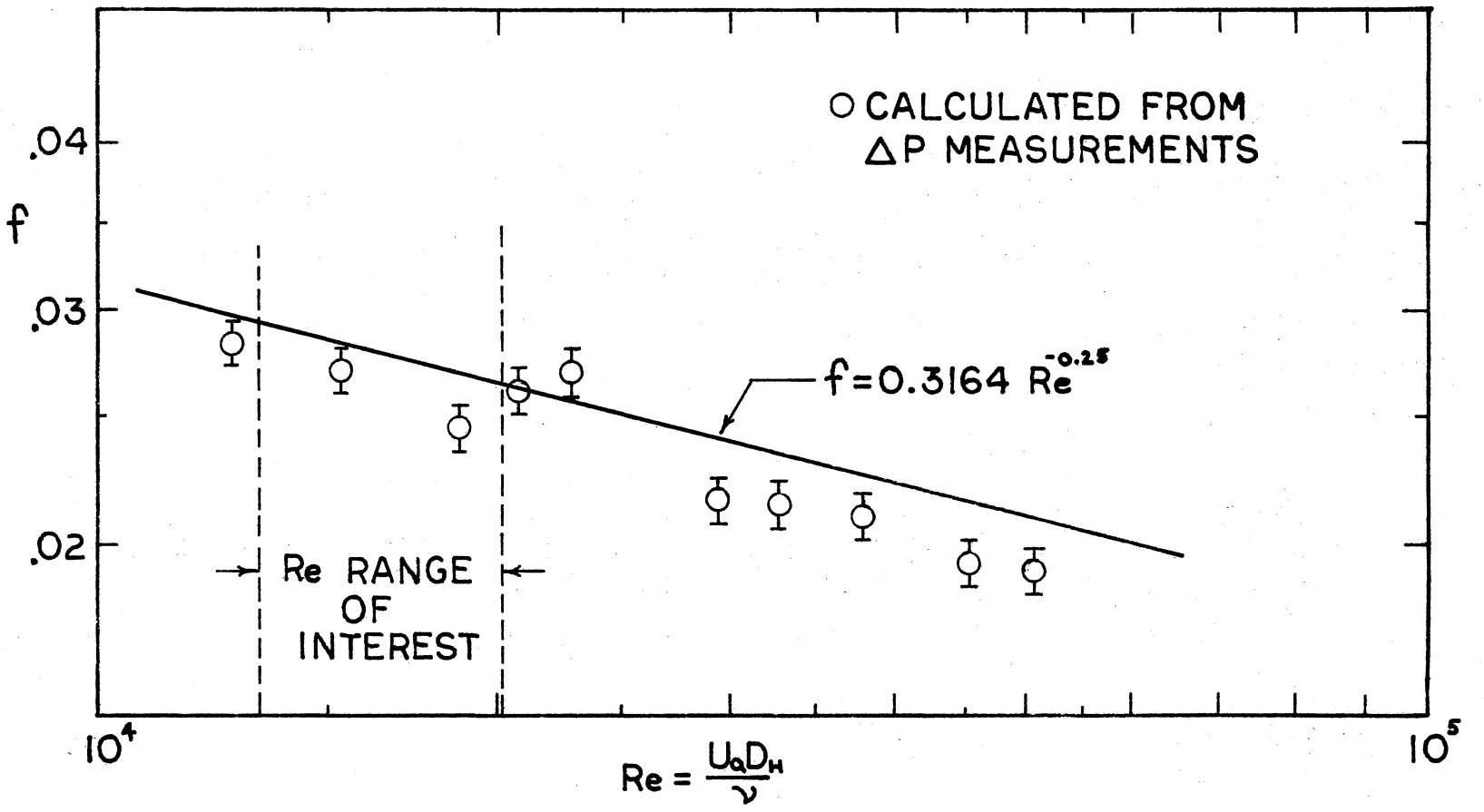

Figure 5. Friction Factor Correlation

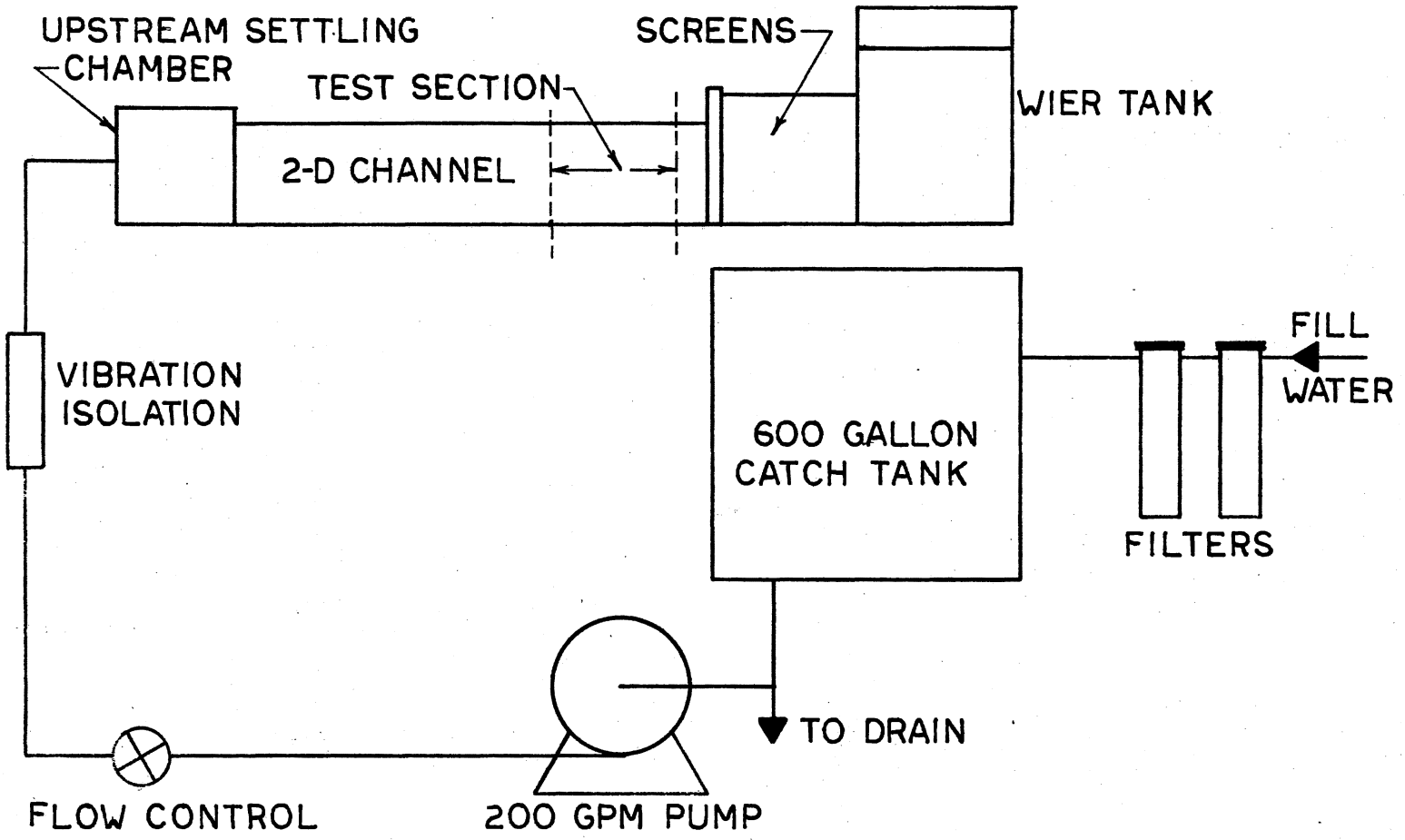

Figure 6. Flow Facility

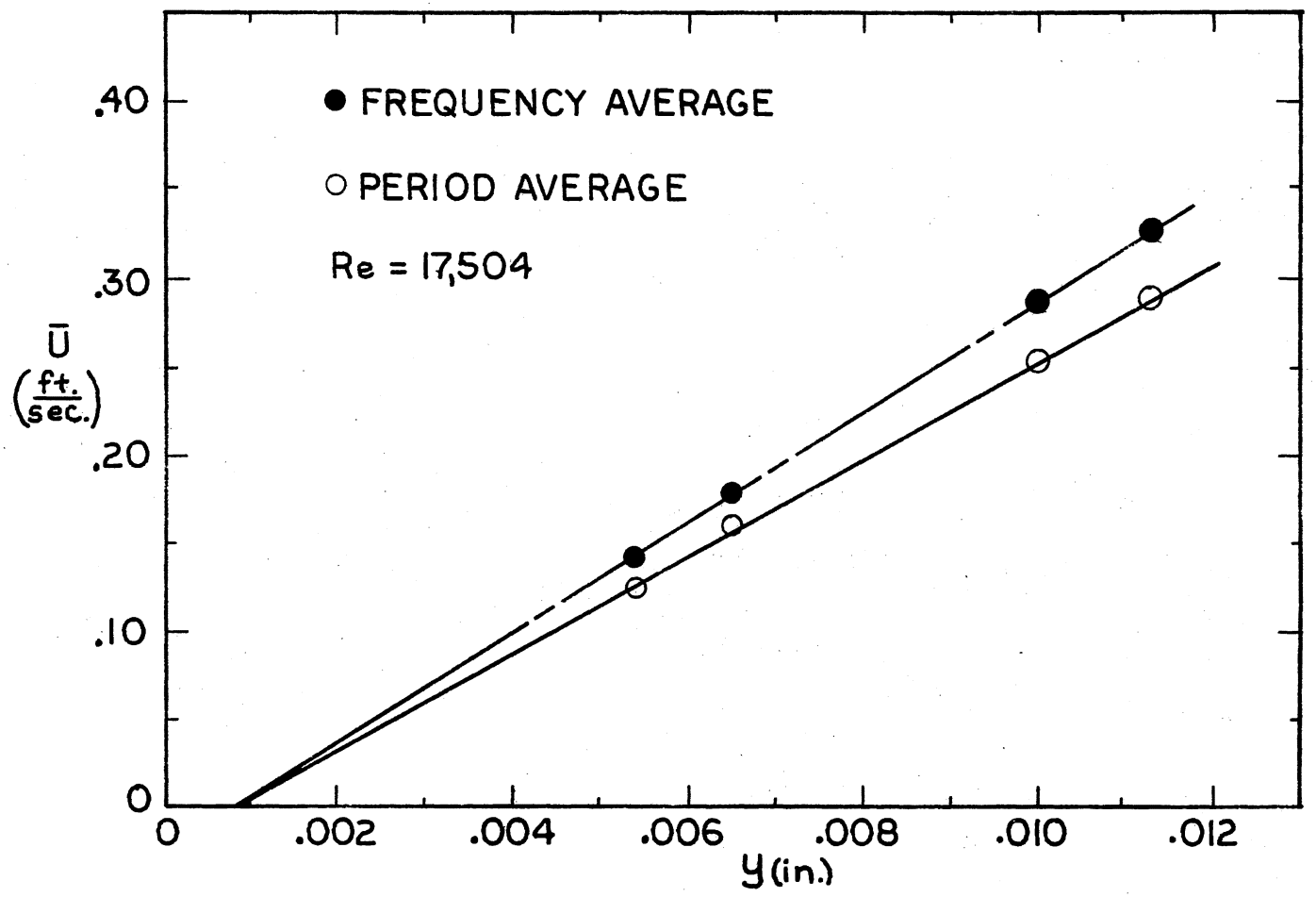

Figure 7. BC-3 Mean Velocity Profile Unshifted by Axis

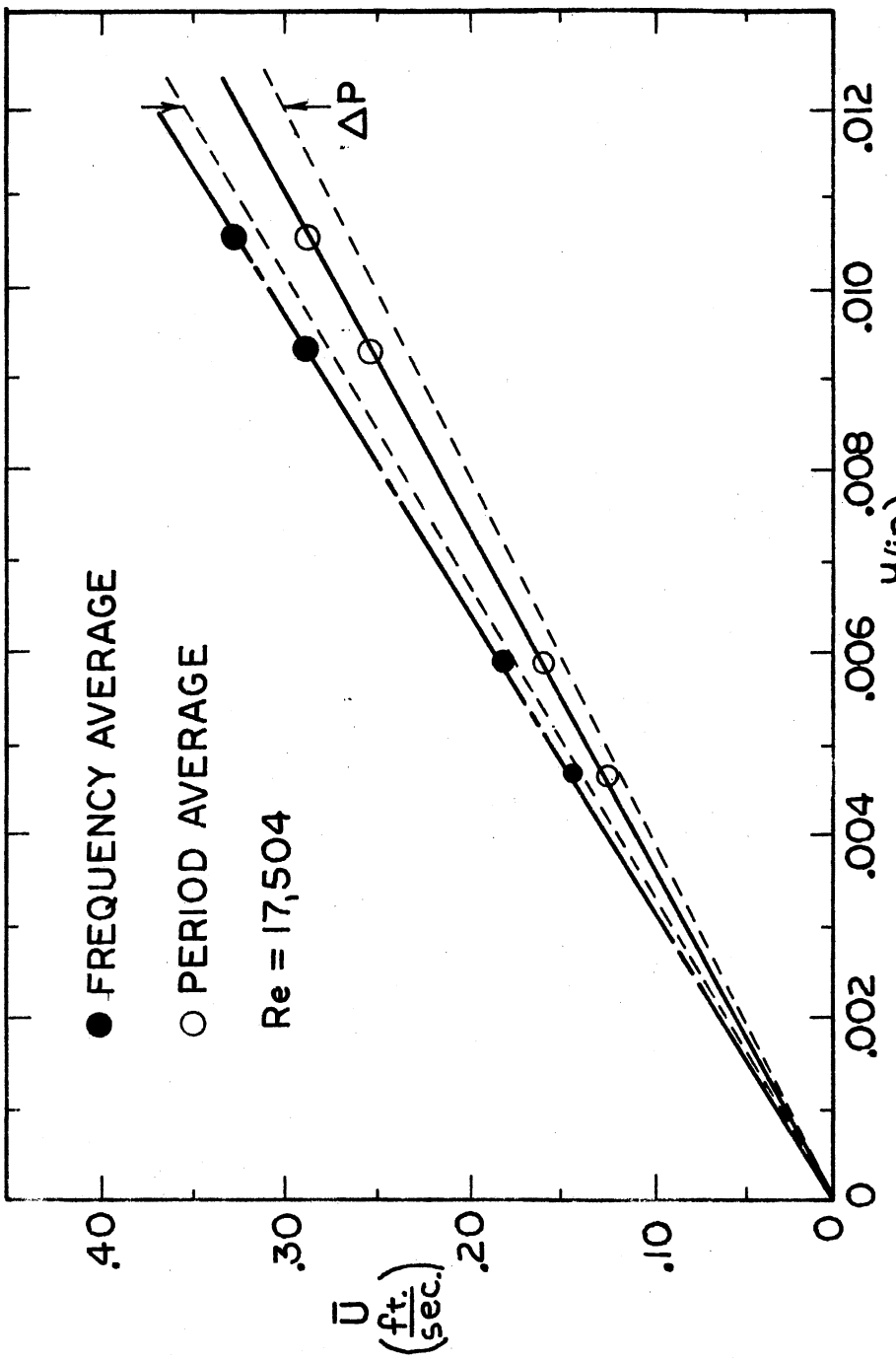

Figure 8. BC-3 Mean Velocity Profile

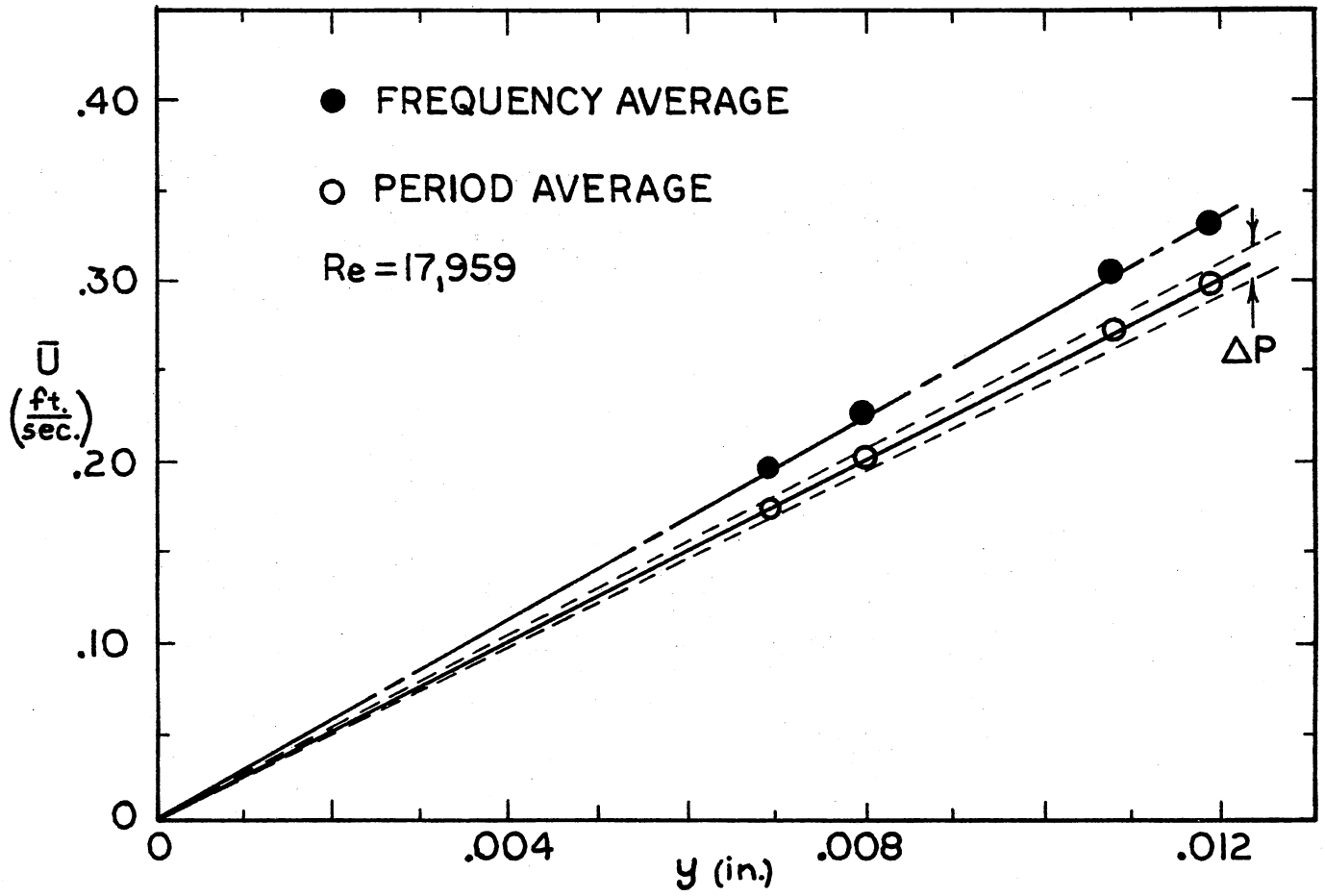

Figure 9. BC-5.2 Mean Velocity Profile

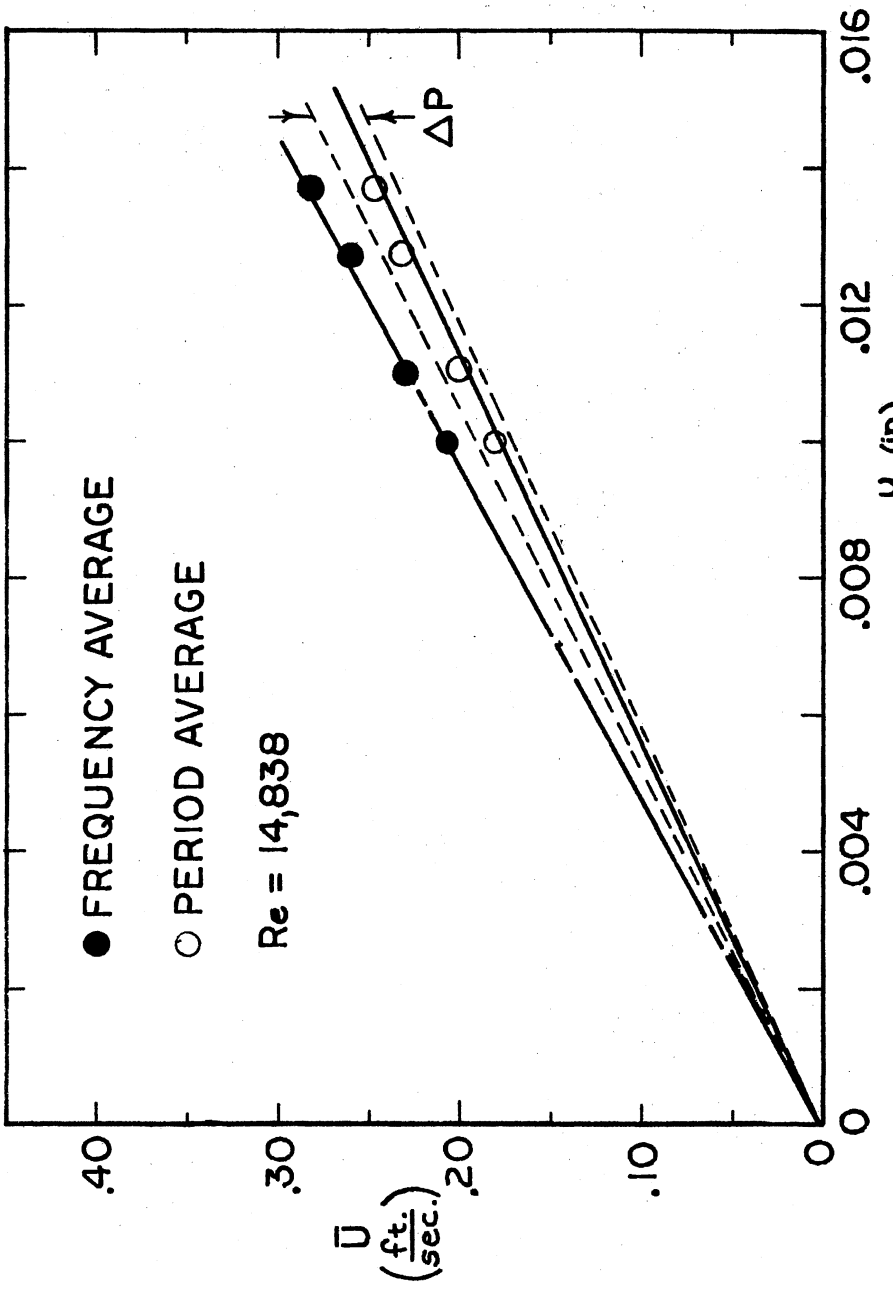

Figure 10. BC-6 Mean Velocity Profile

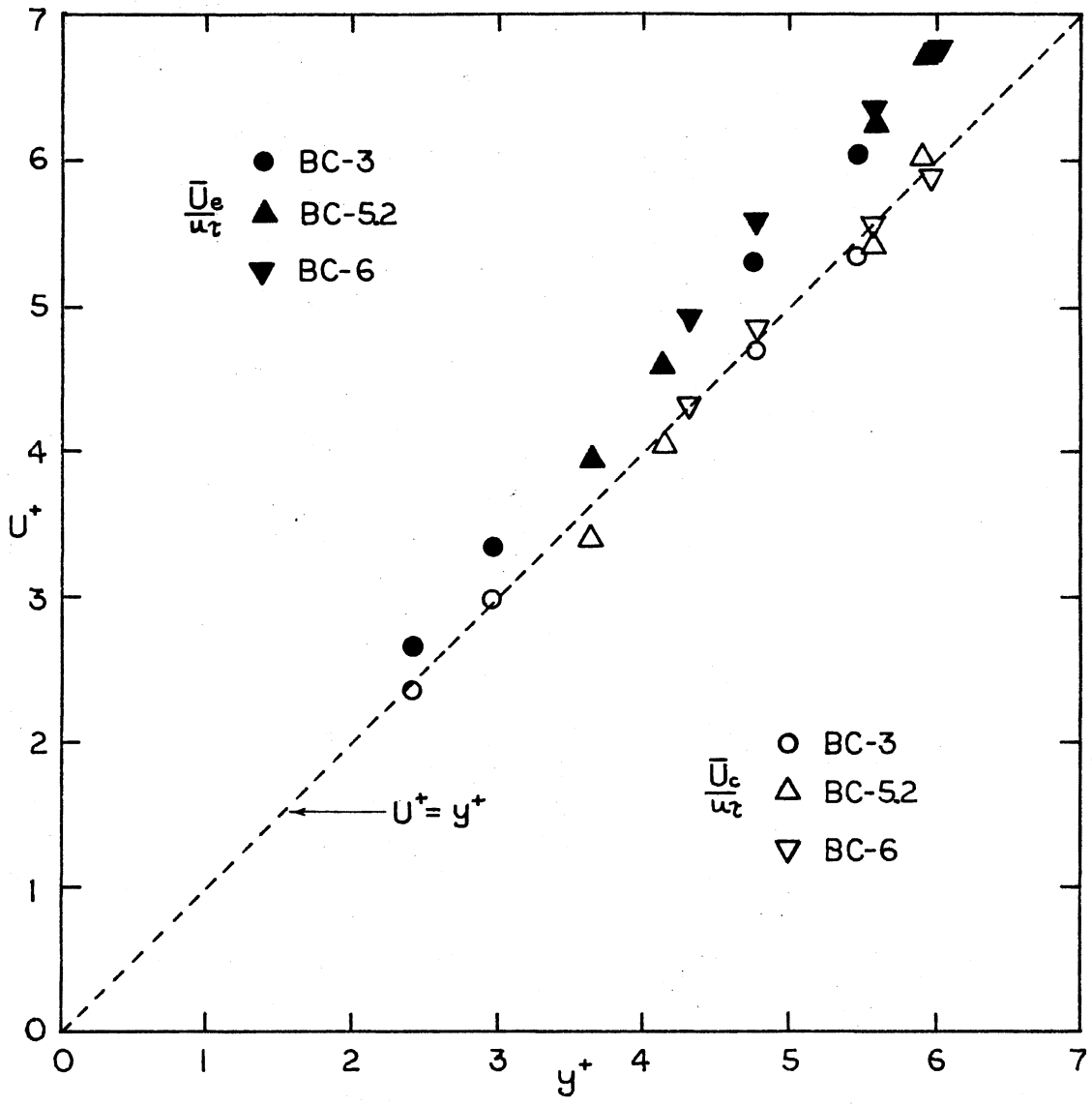

Figure 11. Mean Velocity Profile, Law of the Wall Coordinates

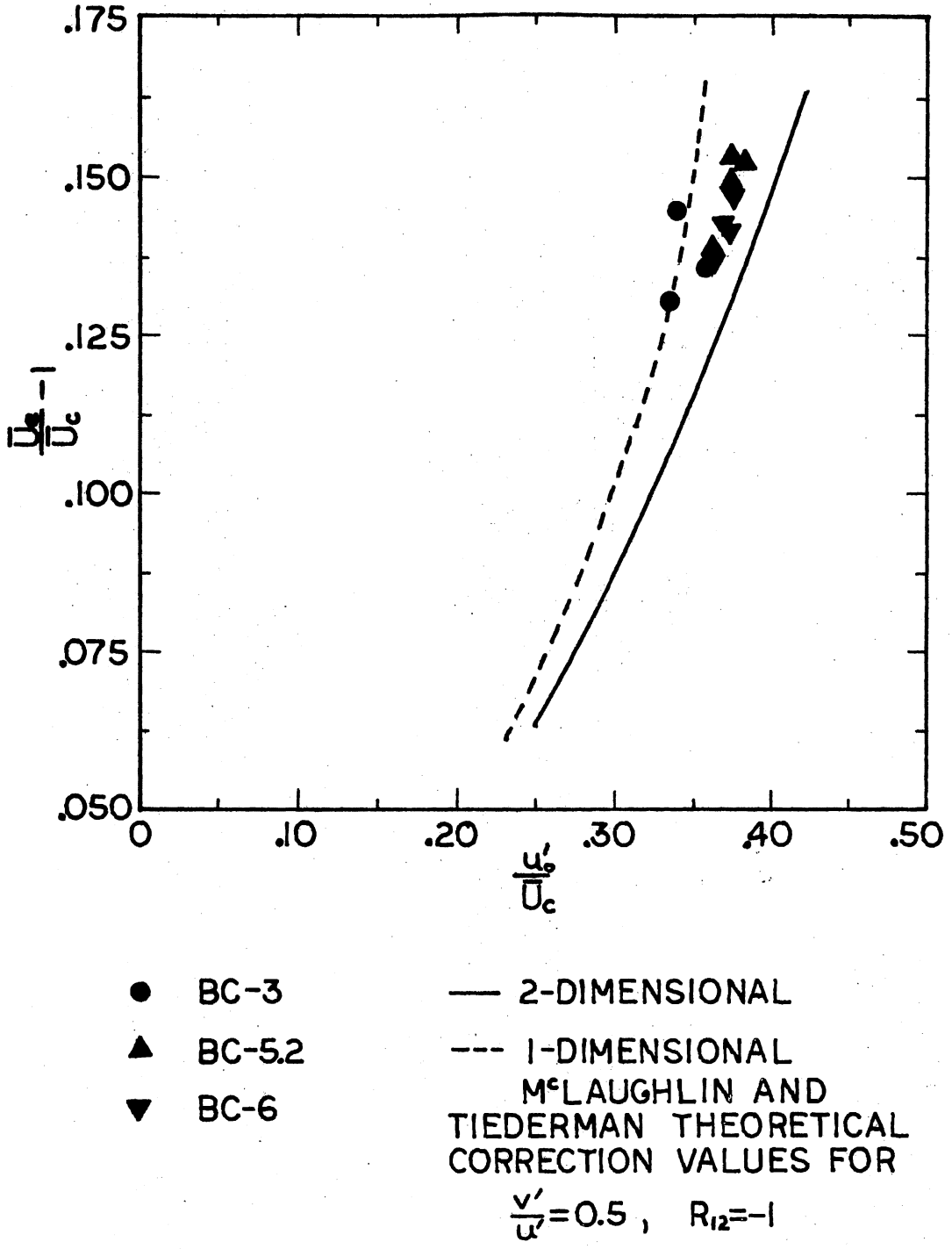

Figure 12. Amount of Sampling Bias Errors for Mean Velocity $\overline{U}$

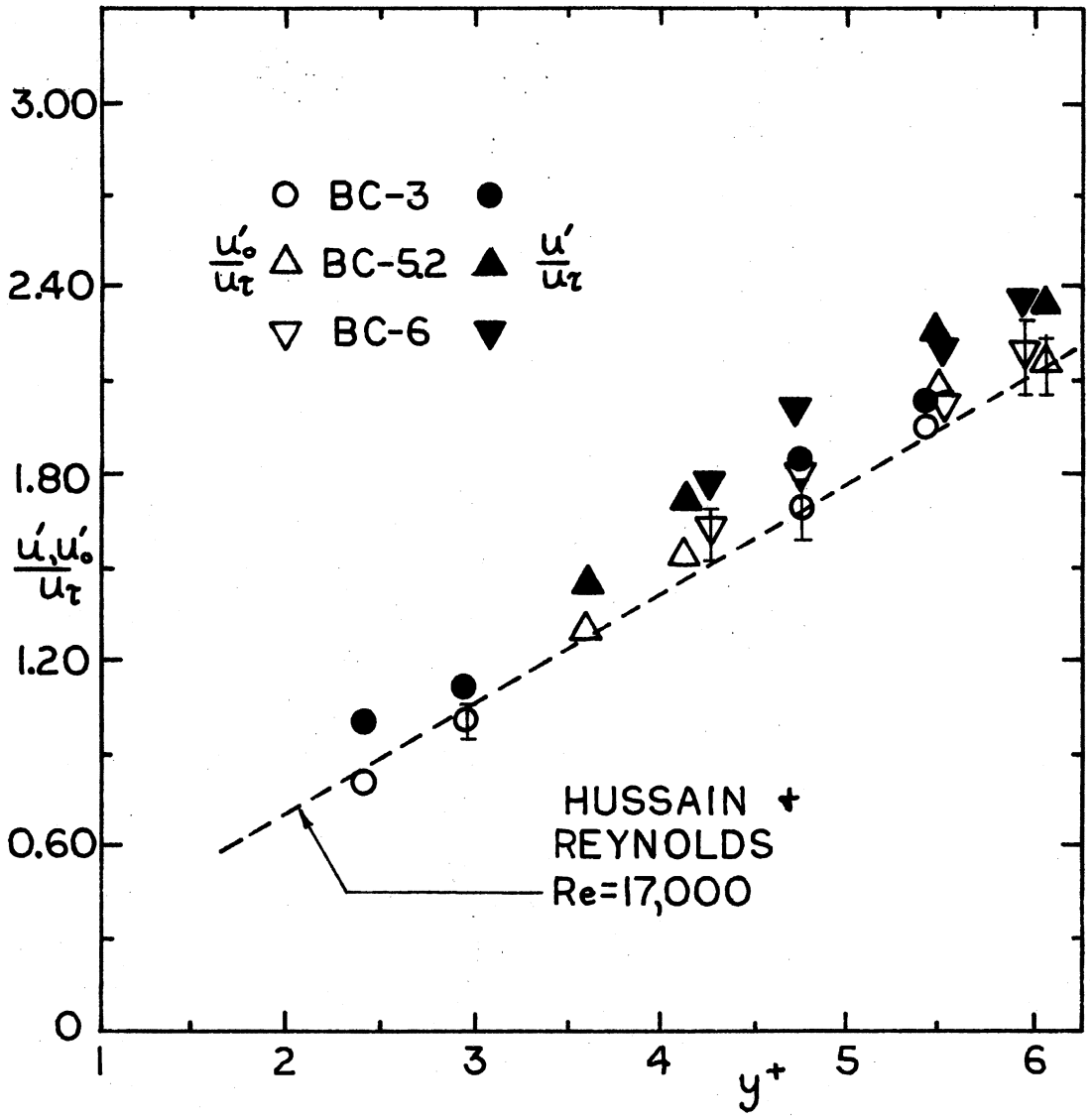

Figure 13. Turbulent Intensities Based on Shear Velocity

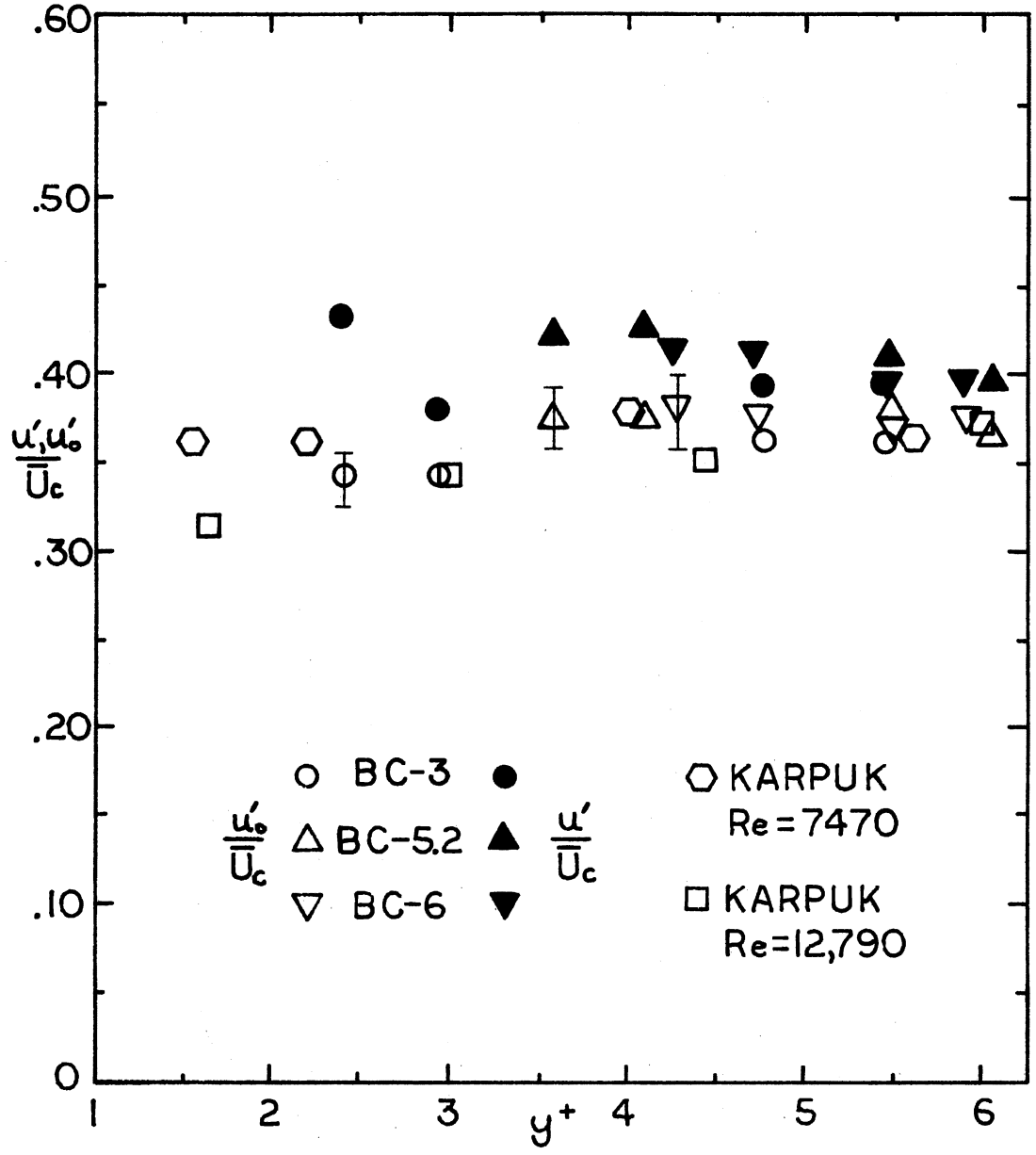

Figure 14. Turbulence Intensities Based on Period Average Mean Velocity

VITA

Michael Scott Quigley

Candidate for the Degree of

Master of Science

Thesis: EXPERIMENTAL EVALUATION OF SAMPLING BIAS IN INDIVIDUAL REALIZATION LASER ANEMOMETRY

Major Field: Mechanical Engineering

Biographical:

Personal Data: Born in Enid, Oklahoma, January 20, 1952, the son of Mr. and Mrs. Bill D. Quigley.

Education: Graduated from Enid High School, Enid, Oklahoma, in May, 1970; received the Bachelor of Science degree in Mechanical Engineering from Oklahoma State University in May, 1974; completed requirements for the Master of Science degree at Oklahoma State University in December, 1975.

Professional Experience: Research engineer, Halliburton Mechanical Research and Development, Duncan, Oklahoma, 1974; graduate teaching-research assistant, School of Mechanical and Aerospace Engineering, Oklahoma State University, 1974-75.

Professional Organizations: AIAA, ASME, Pi Tau Sigma, and Oklahoma Society of Professional Engineers.